Antiretroviral Therapy Does Not Restore Brain Lipids During SIV Infection: Regional Analysis of Metabolic Homeostasis and Depletion

Cory J. White[1#], Andrew M. Gausepohl[1#], Herana Kamal Seneviratne[2,3], Namandjé N. Bumpus[2,4], Dionna W. Williams[1,2,4,5,6*]

[1]Department of Molecular and Comparative Pathobiology, [2]Department of Pharmacology and Molecular Sciences, [3]Department of Chemistry and Biochemistry, University of Maryland Baltimore County, Baltimore, Maryland 21250, [4]Department of Medicine, Division of Clinical Pharmacology, Johns Hopkins School of Medicine, Baltimore, Maryland 21205
[5]Department of Neuroscience, Johns Hopkins School of Medicine, Baltimore, Maryland 21205
[6]Department of Molecular Microbiology & Immunology, Johns Hopkins School of Public Health, Baltimore, Maryland 21205

[#]Authors contributed equally

*Address correspondence to**: Dionna W. Williams, Ph.D.,** Department of Molecular and Comparative Pathobiology, Johns Hopkins University School of Medicine, 733 N. Broadway St., Miller Research Building 849, Baltimore, MD 21205, Email: dwill201@jhmi.edu

ABSTRACT

Human immunodeficiency virus infection (HIV) continues to promote neurocognitive impairment, mood disorders, and brain atrophy even in the modern era of viral suppression. Brain lipids are vulnerable to HIV-associated energetic strain and contribute to HIV-associated neurologic dysfunction due to alterations in lipid breakdown and structural lipid composition. HIV neuropathology is region dependent, yet there has not been a comprehensive spatial evaluation of brain lipids during infection that may impact neurologic function. To address this gap, we evaluated brain lipid distribution using matrix laser desorption/ionization imaging mass spectrometry (MALDI-IMS) across four brain regions (parietal cortex, midbrain, thalamus, and temporal cortex), as well as kidney for a peripheral tissue control, in a virally suppressed simian immunodeficiency virus (SIV)-infected rhesus macaque. We assessed lipids indicative of fat breakdown (acylcarnitines) and critical structural lipids (phosphatidylcholines and phosphatidylethanolamines) across fatty acid chain lengths and degrees of unsaturation. Acylcarnitines with very long-chain, polyunsaturated fatty acids were more abundant across all brain regions than shorter chain, saturated or monounsaturated species. We observed two distinct brain lipid distribution patterns for acylcarnitines and phosphatidylcholines. However, no clear expression patterns emerged for phosphatidylethanolamines. Surprisingly, acylcarnitines were largely missing in kidney, while common phosphatidylcholines and phosphatidylethanolamines were absent in kidney. Overall, our study provides substantial evidence for persistent bioenergetic changes to the brain despite viral suppression, including region-dependent mobilization of acylcarnitines for oxidation and disparities in the presence of key phospholipids necessary for maintaining proper brain structure and function. These data indicate that region-specific interventions to restore proper lipid metabolism are essential for treating HIV neurologic disease in the era of ART.

52 **INTRODUCTION**

53 Human immunodeficiency virus (HIV) continues to pose a significant risk to neurologic
54 health, despite increased life expectancy and quality of life afforded by antiretroviral therapy
55 (ART)-mediated viral suppression (*1*). While the severity of neurologic disease has decreased in
56 the ART era, virally suppressed people with HIV are living long enough to age with the virus and
57 are more susceptible to neurocognitive impairment, mood disorders, and brain atrophy
58 compared to uninfected individuals (*2*, *3*). HIV induces considerable bioenergetic strain to the
59 brain, which is a substantial driver of the neurologic dysfunction that persists despite viral
60 suppression. Lipids are particularly vulnerable to this energetic strain, due to their high
61 abundance and unique composition in the brain, which contributes substantially to neurologic
62 decline when homeostasis of structural lipids are disrupted or the capacity for lipid utilization is
63 decreased (*2*, *3*). Therefore, it was not surprising when strong associations were found between
64 the development of neurocognitive and mood disorders in people with HIV and disruptions in
65 brain lipid metabolism (*4*–*18*). For example, post-mortem brain tissues from people with HIV that
66 experienced cognitive decline were enriched in sphingomyelin containing very long-chain
67 polyunsaturated fatty acids in parietal cortex, medial frontal gyrus, and cerebellum (*18*). In
68 primary astrocyte cultures, brain cholesterol biosynthesis gene expression and brain cholesterol
69 abundance were both decreased by the HIV viral protein, Tat (*19*). Further, Tat increased fatty
70 oxidation gene expression in primary astrocytes (*20*). Another viral protein, gp120, had a similar
71 effect in hippocampal neurons, where it increased sphingolipids containing very long-chain
72 polyunsaturated fatty acids (*18*). These same very long-chain polyunsaturated fatty acid
73 containing phospholipids were also enriched in the brain of transgenic rats that overexpressed
74 regulatory and accessory HIV proteins (*21*, *22*). These studies clearly demonstrate the
75 contribution of lipid dysregulation to central nervous system dysfunction during HIV. However,
76 previous *in vivo* and *ex vivo* studies focused exclusively on profiling total lipid abundance using
77 brain homogenate, without consideration of the spatial differences inherent in the lipid profile

78 (*18*, *21*). This is a major limitation as it is well described that lipid distribution is not uniform
79 across brain regions (*23*, *24*), which likely occurs due to the region-specific expression of lipid
80 breakdown genes and regional differences in structural lipid composition (*25*, *26*). Similarly,
81 region-dependent neuropathological hallmarks of HIV are well recognized to occur, where
82 certain brain regions are preferentially vulnerable to HIV-induced damage and others remain
83 spared (*4*–*15*). For example, areas of the cortex and the basal ganglia are more prone to white
84 matter atrophy while areas of cortex and thalamus are prone to gray matter loss due to infection
85 (*4*, *15*). Despite strong evidence of region-dependent HIV neuropathology and sub-anatomic
86 heterogeneity inherit in lipid metabolism, there have been no studies to date that characterized
87 brain lipid distribution across multiple regions after infection.

88 Therefore, our goal was to characterize lipid distribution in brain utilizing a virally
89 suppressed model reflective of the modern landscape of HIV treatment to evaluate the direct
90 contribution of ART in restoring HIV-induced lipid alterations. We evaluated key lipids indicative
91 of fatty acid breakdown and structural membrane lipid homeostasis using a virally suppressed
92 SIV-infected rhesus macaque model using matrix assisted laser desorption/ionization imaging
93 mass spectrometry (MALDI-IMS). Of importance, this model allows for the direct evaluation of
94 the capacity for ART to restore HIV-induced brain lipid dysregulation in the absence of comorbid
95 disease or dietary and activity differences, which is a substantial confounding factor when
96 performing human studies. We also evaluated lipids in kidney to serve as a peripheral control
97 with known HIV pathology as altered lipid utilization is associated with kidney injury during HIV
98 (*27*). We first assessed acylcarnitines, fatty acid derivatives transiently generated during long-
99 chain fatty acid β-oxidation (**Fig. 1A**) (*23*). We also characterized phosphatidylcholines (**Fig. 1B**)
100 and phosphatidylethanolamines (**Fig. 1C**), prominent phospholipids that are integral in
101 comprising membranes necessary for maintaining cellular composition, integrity, and function

102 (*26*). Species from these lipid classes contain fatty acids with a wide range of chain lengths and
103 degrees of unsaturation that impact physical properties and signaling roles.
104 In this study, we determined that viral suppression afforded by ART was not sufficient to
105 restore brain lipid deposition to levels anticipated in the absence of HIV/SIV. Further, we
106 identified distinct lipid distribution patterns across diverse brain regions that varied according to
107 fatty acid chain length and degree of unsaturation. Very long chain acylcarnitines were more
108 abundant in midbrain, thalamus, and temporal cortex. Similar trends occurred for long-chain
109 saturated and monounsaturated phosphatidylcholines, which had the greatest enrichment in the
110 same three brain regions. Surprisingly, parietal cortex was depleted in both
111 phosphatidylcholines and phosphatidylethanolamines. Unexpectedly, we identified prominent
112 gaps in lipid enrichment across multiple lipid species in diverse brain regions, wherein lipids
113 were completely depleted from the brain tissue and essentially undetectable. Of note, this did
114 not occur throughout the entirety of the tissue section, and lipid enrichment often occurred in an
115 area directly adjacent to the region unpredictably devoid of lipids. These findings demonstrate
116 that lipid dysregulation continue to occur in people with HIV and suggest that altered abundance
117 of these lipids critical to normal brain function contribute to HIV CNS persistence in current the
118 ART era. Overall, this study demonstrates the need for targeted therapeutics to restore region-
119 specific changes in lipid metabolism linked to neurologic decline in people living with HIV.

120 **MATERIALS AND METHODS**

121 **Animal Ethics Statement** All procedures were performed in accordance with the *NIH's Guide*
122 *for the Care and Use for Laboratory Animals,* the *US Department of Agriculture Animal Welfare*
123 *Act*, and under the approval of the Johns Hopkins Medical School Animal Care and Use
124 Committee. The rhesus macaque used for this study was housed in a cage that was appropriate
125 for both size and weight in accordance with federal animal welfare regulation; 1 occupied a 9.0-
126 ft^2 stainless-steel perk bars cage. This animal was included in other studies that included blood
127 and cerebrospinal fluid (CSF) collections and ART injections performed between 8 and 12 a.m
128 (*28*). In those studies, the macaques was anesthetized with ketamine hydrochloride to induce
129 sedation while retaining physiological homeostasis for blood and CSF collections. The macaque
130 was monitored to ensure there were no signs of pain or distress. Criteria for human euthanasia
131 prior to planned endpoint if any of the following were observed: a) weight loss of greater than
132 15%, b) CD4+ T-lymphocytes count less than 5% baseline level, c) clinical signs of neurological
133 disease, d) intractable diarrhea, and opportunistic infection.

134

135 **SIV-infected Rhesus Macaque Model**

136 We used a well-established SIV-infected rhesus macaque (*Macaca mulatta*) model optimal for
137 studying brain pathology, immunological compromise, viral replication, and the impact of
138 therapeutics on HIV outcome (*28–43*). This study was conducted using historical samples
139 originally harvested from one juvenile 4-year-old, 6.1 kg SIV-infected, ART-treated rhesus
140 macaque male (*28*). The macaque wase inoculated intravenously using SIVmac251 as
141 previously described (*28*, *29*). Two weeks after SIV infection, the rhesus macaque was treated
142 with daily intraperitoneal injections of combined ARTs consisting of TFV (20 mg/kg), DTG (25
143 mg/kg), and FTC (50 mg/kg). ARTs were donated from Gilead, ViiV Healthcare, Bristol-Meyers
144 Squibb, Merck, Abbvie, Janssen, and Roche.

145

146 **Quantitation of viral load in plasma and CSF**

147 SIV was assessed in plasma and CSF as previously described (*28*, *44–47*). Briefly, RNA was
148 isolated from 140 µL of plasma or CSF using the QIAamp Viral RNA Mini kit (Qiagen) in
149 accordance with the manufacturer's protocol with the modification of on-column DNase
150 digestion (RNase free DNase kit; Qiagen) using RQ1 RNase free DNase (Promega) in the
151 enzyme mix. Quantification of SIV RNA was performed by reverse transcription polymerase
152 chain reaction (qRT-PCR) using the following primers and probes: FWD-(SGAG21) 5′-
153 GTCTGCGTCATCTGGTGCATTC-3′; REV-(SGAG22) 5′-
154 CACTAGGTGTCTCTGCACTATCTGTTTTG-3′, probe (pSGAG23) 5′-
155 (FAM)CTTCCTCAGTGTGTTTCACTTTCTCTTCTG-(BH1)-3′.

156

157 **Necropsy and Harvest**

158 At approximately 130 days post inoculation, the juvenile SIV-infected, ART-treated rhesus
159 macaque male was sacrificed in accordance with federal guidelines and institutional policies
160 (*28*). Necropsy protocols were performed in accordance with previous work routinely performed
161 within the Retrovirus Laboratory of the Department of Molecular and Comparative Pathobiology
162 in accordance with the American Veterinary Medical Association guidelines for euthanasia of
163 animals (*28*, *29*, *46*, *48*). Euthanasia occurred with an overdose of sodium pentobarbital while
164 under ketamine sedation (15- to 20- mg/kg intramuscular injection) before perfusion with
165 phosphate-buffered saline (PBS) (Gibco) to remove blood from tissues as described (*28*, *29*, *46*,
166 *48*). After harvest, the whole brain was placed in cold 2.5% agarose, and 4mm coronal sections
167 were obtained; fresh kidney was cut into four sections horizontally. Brain regions (parietal
168 cortex, temporal cortex, thalamus, and midbrain) and kidney were fresh frozen using liquid
169 nitrogen in optimum cutting temperature medium (OCT) (Sakura Finetek Inc, Torrance, CA) and
170 stored at -80°C until cryosectioning (*29*).

171

172 **Materials & Chemicals for MALDI**

173 MALDI matrix, a-cyano-4-hydroxycinnamic acid (CHCA) was obtained from MilliporeSigma (St.
174 Louis, MO). The CHCA matrix is widely suitable for lipids (*49*). All solvents and other chemicals
175 used were either reagent or high-performance liquid chromatography (HPLC) grade and
176 purchased from Fisher Scientific (Hampton, NH), unless otherwise specified.

177

178 **Tissue Sections & Matrix Application**

179 OCT-embedded brain and kidney were sectioned to 10 μm onto Superfrost Plus Microscope
180 Slides (Fisher Scientific, Pittsburgh, Pennsylvania) at -20°C using a Leica CM3050S cryostat
181 (Leica Biosystems, Buffalo Grove, IL). Matrix [CHCA, 10 mg/ml in ACN:H_2O (50:50, v/v)] was
182 applied to each slide using a TM-Sprayer (HTX Technologies, LLC, Chapel Hill, NC) at a flow
183 rate of 100 mL/min. The TM-Sprayer was operated at an air pressure (N_2) of 10 psi, spray
184 nozzle velocity of 1200 mm/min, track spacing at 2 mm, and spray nozzle temperature at 80°C.
185 Sixteen passes (matrix deposition cycles) were employed for homogeneous deposition of matrix
186 onto each slide.

187

188 **MALDI Imaging**

189 MALDI-MSI data were acquired using a LTQ Orbitrap XL (Thermo Fisher Scientific, Bremen,
190 Germany), equipped with a Fourier transform mass spectrometer (FTMS) with the MALDI ion
191 source fitted with a direct beam N_2 laser (l 5 337.7 nm). Data acquisition was performed using
192 the positive ion mode of the MS instrument at a mass range of m/z 100–1000 Da. Mass
193 resolution of the FTMS analyzer was 60,000. CHCA matrix was used at 10 mg/ml for ionization
194 of lipids and the laser energy of 7.8 mJ was used. The camera from the MALDI instrument was
195 used to define regions of interest and generate MALDI position files. Ion images had a spatial
196 resolution of 50 μm. Mass spectrometry data processing and analysis were done using Xcalibur

197 3.0 (ThermoFisher Scientific) and ion images were generated using ImageQuest 1.0.1 software
198 (Thermo Fisher Scientific, San Jose, CA).
199
200 **Selection of Ion Images**
201 Representative lipid ion images were selected for known m/z values of multiple species for the
202 following lipid classes: acylcarnitines, phosphatidylcholines, and phosphatidylethanolamines
203 using Xcalibur 3.0 (ThermoFisher Scientific) (*50*). Ion values were determined for H^+, K^+, and
204 Na^+ adducts from each neutral lipid using LIPID MAPS Lipidomics Gateway mass (m/z)
205 calculation tool for lipid classes. Representative images were selected upon determination of
206 uniform expression patterns from all three adducts.
207
208
209

RESULTS

Virally suppressed, SIV-infected macaque model

We utilized a virally suppressed rhesus macaque model because of the experimental control it facilitates that limit confounding factors inherent with postmortem human brain (*28*, *51–54*). One juvenile male rhesus macaque was infected with SIVmac251 for 14 days, followed by 90 days of viral suppression. We showed that this model achieved peak viremia at 14 days post inoculation and accomplished complete viral suppression by day 42 post inoculation (28 days after ART initiation) (*28*). Upon necropsy, perfusion was performed, and the brain and kidney were harvested for lipid analysis via MALDI-IMS (*18*).

Determination of lipid spatial distribution in a virally suppressed, SIV-infected macaque

Brain lipids are necessary for maintaining structure, propagating action potentials, use as signaling molecules, and as a source of energy (*3*, *23*, *55*). Numerous neurocognitive disorders, mood disorders, and neurovirulent diseases, including HIV, are linked to dysregulated lipid metabolism (*17*, *56–58*). HIV viral proteins decrease brain cholesterol and sphingolipid abundance and the expression of enzymes necessary for their biosynthesis (*18*, *19*). HIV viral proteins also disrupted membrane lipid homeostasis when overexpressed in rats (*21*). However, previous studies failed to examine a component critical to lipid abundance and function: region-specific metabolic profiles necessary to meet energetic demands, supply structural needs, and maintain metabolic homeostasis.

To address this gap in knowledge, we evaluated brain lipid distribution by MALDI-IMS from HIV-relevant brain regions (midbrain, parietal cortex, thalamus, temporal cortex) (*4*, *28*). We also performed MALDI-IMS on kidney as a point of reference for lipid distribution in peripheral tissues with known HIV-relevance as renal disorders remain prevalent even among virally suppressed people living with HIV (*59*). To examine lipid regional distribution, 10-μm coronal slices of parietal cortex, thalamus, temporal cortex, midbrain, and kidney were imaged

236 with a 50-μm resolution (**Fig. 1A; Fig. 1B**) using a m/z acquisition range of 100-1000 Da (**Fig**
237 **1A; Fig. 1B**). We focused on three main classes of lipids of key importance to lipid utilization
238 (acylcarnitines) and cellular structure/homeostasis (phosphatidylcholines and
239 phosphatidylethanolamines).
240
241 **Acylcarnitines are abundant in brain, variably expressed in differing regions, and**
242 **minimally present in kidney**
243 We first evaluated acylcarnitines, which have diverse chain lengths that range from two
244 to over twenty carbons with zero to over six degrees of unsaturation (*60*). There was a striking
245 pattern wherein very long-chain acylcarnitines were highly expressed in brain, but minimally
246 present in kidney, which was consistent across all imaged brain regions from our SIV-infected,
247 ART-treated rhesus macaque. This is evidenced by the very long chain acylcarnitine, C22:4,
248 that was highly expressed in brain but marginally detected in kidney (**Fig. 2**). Interestingly,
249 C18:3 was the only acylcarnitine species prominently observed in kidney (**Fig. 2**). Surprisingly,
250 this acylcarnitine was minimally represented in brain.
251 We determined that, while prominently represented, very long-chain acylcarnitines had a
252 high level of regional specificity across brain regions (**Fig. 2**). C20:0 and C22:3 were highly
253 expressed and homogenously distributed in parietal cortex. Yet, they were sparsely abundant in
254 midbrain, localizing only to the perimeter of the tissue (**Fig. 2**). These same acylcarnitines had a
255 distinct localization in thalamus where they were almost uniformly present with incomplete, but
256 prevalent, representation. Similar trends existed for C22:5, which was not present in parietal
257 cortex, but was abundant in both midbrain and thalamus. Interestingly, C22:5 had a unique
258 localization where it had the highest abundance in the innermost portion of tissue but was
259 absent at the outermost edges. C20:1 showed a similar trend in regional specificity where it was
260 homogenously present in parietal cortex but localized only to the central portions of midbrain
261 and thalamus (**Fig. 2**).

262 **Phosphatidylcholines of longer-chain lengths are more prominent in brain than in kidney**

263 We next evaluated phosphatidylcholines, focusing on species with common medium-,
264 long-, and very long-chain acyl groups (**Fig. 3**). Parietal cortex had the lowest enrichment of
265 analyzed phosphatidylcholines, where those of all chain lengths were minimally detected (**Fig.**
266 **3A**). Conversely, phosphatidylcholines were highly expressed and uniformly present in
267 midbrain. Thalamus and temporal cortex had high expression of medium-chain
268 phosphatidylcholines, but lower abundance of the longer chain lengths. Interestingly,
269 phosphatidylcholines had a comparable spatial distribution as some of the acylcarnitines in
270 thalamus, wherein the greatest expression was restricted to the uniquely patterned internal zone
271 (**Fig. 3A; Fig. 2**). The temporal cortex had the most unique and variable phosphatidylcholine
272 localization patterns of all examined brain regions. PC(32:0) and PC(32:1) were abundant in a
273 large, central portion of the temporal cortex, while PC(40:4) localized only to the top portion of
274 the tissue. In contrast, PC(44:6) was primarily only at the bottom portion of the temporal cortex
275 (**Fig. 3A**). Of interest, there was one notable exception that occurred uniformly across brain
276 regions. Very-long chain phosphatidylcholines were lowly expressed in brain (**Fig. 3A**). No clear
277 trend in phosphatidylcholines occurred in kidney, where some species were highly and
278 uniformly expressed, while others were present to a lower extent (**Fig. 3B**).

279

280 **Phosphatidylethanolamines are heterogeneously present in brain and kidney**

281 Phosphatidylethanolamines were the last lipid of investigation. Overall, the spatial
282 distributions of phosphatidylethanolamine species showed less consistent patterning than that
283 which occurred for acylcarnitines and phosphatidylcholines in both brain and kidney (**Fig. 4**).
284 Like phosphatidylcholines, smaller chain phosphatidylethanolamines were more prominent
285 across all brain regions and in kidney, while larger phosphatidylethanolamines were less
286 represented across both tissues (**Fig. 4**). Interestingly, phosphatidylethanolamines were not
287 visible in parietal cortex (**Fig. S1**).

288 **DISCUSSION**

289 Our study is among the first to evaluate the spatial distribution of major lipid classes
290 related to lipid utilization (acylcarnitines) and membrane phospholipid homeostasis
291 (phosphatidylcholines and phosphatidylethanolamines) in brain and kidney by MALDI-IMS in a
292 virally suppressed non-human primate model of HIV infection. We identified distinct lipid
293 distribution patterns lipid distribution for acylcarnitines and phosphatidylcholines, but no well-
294 defined patterns for phosphatidylethanolamines. Acylcarnitines comprised of long-chain
295 polyunsaturated fatty acids were more abundant across all brain regions compared to kidney.
296 However, the distribution pattern within each brain region differed by species, where some
297 species were present along the peripheries of regions and others were restricted to the in
298 interior portions. Phosphatidylcholines containing common saturated and monounsaturated
299 long-chain fatty acids were most abundant across brain regions and in kidney. Surprisingly, the
300 parietal cortex was particularly vulnerable to lipid depletion and lacked both
301 phosphatidylcholines and phosphatidylethanolamines. Our findings demonstrate distinct
302 patterns of lipid distribution, including enrichment of very long chain polyunsaturated
303 acylcarnitines across brain regions and limited phosphatidylcholines in parietal cortex. Further,
304 they indicate that, despite viral suppression, ART is not sufficient to restore HIV-induced
305 dysregulations in brain lipid abundance and composition, where some brain regions are at
306 heightened risk for lipid depletion. This has profound implications for the persistence of HIV
307 CNS disease in the era of ART, identifies a previously unrecognized marker of HIV neurologic
308 dysfunction, and indicates that therapeutically targeting lipid metabolic processes in a region-
309 specific manner will be integral in restoring appropriate neurologic function in people living with
310 HIV. Our innovative approach in evaluating lipid distribution across multiple brain regions was
311 imperative to understand HIV-induced changes in the brain lipidome and demonstrates the
312 importance of spatially profiling lipids, rather than exclusively quantifying lipid concentrations in
313 tissue homogenate (*23*, *25*).

314 HIV viral proteins, which are expressed despite suppression of viral replication, greatly
315 contribute to neurologic dysfunction. These viral proteins contribute to neurotoxicity manifesting
316 as dendritic injuries (*61*–*63*), neurogenic deficits (*64*), and neuroendocrine defects (*65*).
317 Neurotoxic HIV proteins include gp120, gp41, Tat, Nef, Rev, and Vpr (*66*, *67*). Viral proteins
318 alter brain bioenergetics in numerous ways, including Ca^{2+} dysregulation (*68*–*70*), modulated
319 fatty acid oxidation (*20*), and electron transport chain complex abnormalities (*71*). They also
320 disrupt metabolic coupling in the brain (*20*), elevate reactive oxygen species (*72*, *73*), and
321 exacerbate neuroinflammation (*61*, *74*). Previous studies showed that HIV viral proteins
322 increased fatty acid oxidation genes *in vitro* and disrupted the balance of membrane lipids (*20*,
323 *21*). Our findings in this study identify the high abundance of many acylcarnitines during viral
324 suppression. This is of major significance because acylcarnitines are fatty acid oxidation
325 intermediates, which is often contested to occur within brain (*23*). Our studies strongly implicate
326 that the HIV-infected brain undergoes a considerable amount of fatty acid oxidation and is
327 enriched in lipid species associated with countering HIV-associated neuroinflammation. Further,
328 while phosphatidylcholines containing polyunsaturated very long-chain fatty acids are less
329 prominent than phosphatidylcholines containing common saturated and unsaturated long-chain
330 fatty acids, they are still well represented across most brain regions. Previous work determined
331 brain tissue from people with HIV that experienced severe cognitive decline had increased very
332 long-chain fatty acids in sphingolipids, a class of structural membrane lipids, despite viral
333 suppression (*18*). It is possible that elevations in very long-chain, polyunsaturated fatty acids
334 contribute to, or are indicative of, cognitive decline. Determining the mechanisms by which
335 HIV/SIV and viral suppression impact these fatty acids is necessary to identify therapeutic
336 strategies to restore changes to brain lipid homeostasis that contribute to HIV-associated
337 cognitive decline.
338 Chronic inflammation is another major contributor to CNS dysfunction that persists in
339 people living with HIV, even with successful ART (*75*–*77*). Inflammation in the periphery,

340 perivascular space, and within the brain parenchyma contribute to CNS dysfunction during HIV
341 (*78–82*). Chronic inflammation promotes neuropathology, including accelerated brain aging,
342 increased risk of developing psychiatric disorders, and cognitive decline (*83*). In the short term,
343 the neuroimmune response is beneficial by promoting pathogen clearance, inducing
344 angiogenesis, and increasing wound healing (*84*). In addition to canonical cytokines and
345 chemokines, classes of specialized pro-resolving lipid mediators, including lipoxins, protectins,
346 resolvins, and meresins, also promote neuroinflammation (*85*). Our study identified high
347 abundance of the C22:5 fatty acid prominently found in specialized proresolving mediators
348 known to alleviate neuroinflammation in specific areas of midbrain, thalamus, and temporal
349 cortex (**Fig. 2**). This is important because previous studies determined that HIV viral proteins
350 increased the abundance of C22:5 acid in total lipid, phosphatidylethanolamine, and
351 triglycerides (*21*). Our findings indicate that lipid dysregulation in brain that contributes to
352 persistent neuroimmune activation during HIV/SIV-infection, even with adequate viral
353 suppression. It is likely that the high abundance of C22:5 exists to counter the chronic
354 neuroinflammation that occurs after HIV infection.
355 ART may also play a direct role in lipid dysregulation in brain as its adverse impact on
356 metabolism is well characterized. Systemically, it is well established that ART causes a mean
357 weight gain of 3-7 kg within the first year of initiating treatment (*86–89*). Further, specific ART
358 drugs or ART classes can have varying impacts on circulating lipid levels, blood pressure, and
359 risks for developing metabolic syndromes, including diabetes mellitus. For example, classical
360 non-nucleoside reverse transcriptase inhibitors and protease inhibitors were known for greatly
361 increasing the likelihood of developing dyslipidemia (*90*). Even though newer antiretrovirals do
362 not elevate circulating lipids to the same extent, tenofovir prodrugs, including tenofovir
363 alafenamide, increase cholesterol species (*91*). This occurs despite the known impact of HIV on
364 diminishing total cholesterol levels (*86*, *92–95*). Conversely other ARTs, including raltegravir,
365 dolutegravir, and bictegravir, have either a beneficial or minimal impact on the cholesterol profile

366 after changing regimens from older protease inhibitors (*86*, *96*). Hypertension, another disorder
367 related to lipid dysregulation, is also more prevalent in individuals receiving ART. There is a
368 1.68-fold higher risk of developing hypertension in people living with HIV on ARTs in
369 comparison to those not on ART (*86*, *97*). However, it is not well characterized whether many of
370 these changes to metabolic parameters occur due to the antiretrovirals directly, or because of
371 the weight gain associated with many ARTs (*86*). With the clear role of ART in promoting
372 lipodystrophy and metabolic dysfunction systemically, it is likely that similar perturbations also
373 occur in brain.

374 Indices of kidney injury due to HIV are common as virally suppressed people living with
375 HIV are aging. However, ART also poses a direct insult to kidney physiology. For example,
376 tenofovir and its adenofir analog induced mitochondrial dysfunction and glycogen accumulation
377 in human kidney cells that may contribute to nephrotoxicity (*98*). While less is understood about
378 the impact ART on lipid metabolism in kidney, tenofovir decreased levels of low-density
379 lipoprotein and increased the rate of change in urine-liver-type fatty acid binding
380 protein/creatinine. These are known markers of elevated risk of hyperlipidemia and chronic
381 kidney disease respectively (*99*), demonstrating a precedence for ART promoting lipid
382 dysregulation in kidney. The contribution of ART to lipid perturbations in kidney has profound
383 implications for people with HIV as lipid metabolism is highly relevant to kidney health, as it is
384 the organ that preferentially oxidizes fatty acids used for energy. Further, lipid metabolism
385 dysfunction is a well-established risk factor for kidney disease (*27*). Despite the clear
386 importance and relevance of lipids in kidney function and normal physiology, we detected only a
387 single acylcarnitine species in kidney (C18:3) (**Fig. 2**). It is possible that the acylcarnitine
388 species we did not detect were exhausted to generate ATP, or that defective mitochondrial
389 metabolism occurred that prevented other acylcarnitines from being produced (*98*). Our findings
390 demonstrate that the kidney remains vulnerable to lipid dysfunction, even in the setting of ART-

391 mediated viral suppression, and HIV/SIV and ART may contribute to increased propensity for
392 kidney injury due to lipid dysregulation.

393 HIV poses a major risk to brain lipid metabolic homeostasis that contributes to
394 neurologic decline and brain pathology that continue to occur, despite viral suppression (*4–18*).
395 Characterizing region-dependent changes in lipid profiles is critical for determining region-
396 specific interventions that will restore proper brain function and metabolism disrupted due to HIV
397 CNS disease. We utilized advancements in lipid imaging by MALDI-IMS combined with our
398 virally suppressed SIV rhesus macaque model for an innovative approach to address this gap.
399 Here, we demonstrated that, despite viral suppression, lipids indicative of increased fatty acid
400 oxidation, dysregulated structural lipids, and activated neuroimmune response were prominent
401 in a SIV-infected non-human primate. These metabolic changes occurred in a region-dependent
402 manner, and it is imperative to fully understand HIV-induced changes to the brain lipidome that
403 may contribute to HIV-associated neurologic decline in order to develop therapeutics that target
404 spatially distinct areas of brain metabolic dysfunction.
405
406
407

Acknowledgements

We thank the members of the Johns Hopkins School of Medicine Retrovirus Laboratory in the Department of Molecular and Comparative Pathobiology for husbandry of non-human primate models, analysis of infection and viral suppression of the animal, necropsy and sample collection, and for veterinary care including Suzanne E. Queen, Erin N. Shirk, Brandon T. Bullock, Kelly A. Metcalf Pate, Lisa M. Mangus, Janice E. Clements, and Joseph L. Mankowski. We are also thankful for Gilead and ViiV for graciously providing antiretrovirals used by non-human primate models.

This study was supported by National Institutes of Health (NIH) grants R00 DA044838 and R01 DA052859 to Dionna W. Williams, U19AI113127 to Namandjé N. Bumpus, and K00 NS118713 Cory J. White. Also, this work was in part supported by pilot funding provided by parent funding under the JHU NIMH Center for Novel Therapeutics for HIV-associated Cognitive Disorders P30 MH075673 to Justin C. McArthur, and P01 AI131306 to Janice E. Clements.

Images in figures were created using BioRender.

Conflict of Interest

The authors report no conflicts of interest.

Author Contributions

D.W.W. and C.J.W. performed experiments, A.M.G. and C.J.W. analyzed data, D.W.W. and C.J.W. were responsible for conceptualization of the study design, H.K.S. and N.N.B. developed the methodologies, C.J.W. and D.W.W. wrote the original draft with review and editing from all authors.

432 **FIGURE LEGENDS**

433

434 **Figure 1. MALDI MS Imaging of SIV-infected, ART-treated macaque tissues using CHCA**
435 **matrix and positive mode of the LTQ Orbitrap XL instrument.** Representative full scan
436 spectra and images of total ion counts of SIV-infected, ART-treated rhesus macaque A) brain
437 regions: (parietal cortex, midbrain, thalamus, and temporal cortex) and B) kidney. Red signifies
438 the highest intensity and blue the lowest of each m/z. C) Acylcarnitine (red), phosphatidylcholine
439 (blue), and phospatidylethanolamine (gray) structures. R = acyl (fatty chain) group.

440

441 **Figure 2. Very long-chain acylcarnitines are prevalent in the brain, but not kidney, where**
442 **spatial distribution varies by species composition.** Representative MALDI-IMS of SIV-
443 infected, ART-treated rhesus macaque brain regions [parietal cortex (P. ctx), midbrain,
444 thalamus, and temporal cortex (T. ctx)] and kidney of A) very long-chain polyunsaturated AC
445 C22:4 species, B) polyunsaturated C18:3 AC species, C) varying very long-chain un-, mono-,
446 and polyunsaturated AC species demonstrating differences in spatial distribution. Red signifies
447 the highest intensity and blue the lowest of each m/z.

448

449 **Figure 3. Lower chain-length phosphatidylcholines are more abundant in both kidney**
450 **and across brain regions.** Representative MALDI-IMS of SIV-infected, ART-treated rhesus
451 macaque brain regions of A) m/z values shared by representative PCs of similar chain length in
452 A) the following brain regions: parietal cortex (P. ctx), thalamus, temporal cortex (T. ctx), and
453 midbrain as well as B) in kidney. Red signifies the highest intensity and blue the lowest of each
454 m/z.

455

456

457 **Figure 4. Patterns in phosphatidylethanolamine spatial distribution across brain regions**
458 **or within a respective tissue are less clear.** Representative MALDI-IMS of SIV-infected, ART-
459 treated rhesus macaque brain regions of A) m/z values shared by representative PEs of similar
460 chain length in A) the following brain regions: thalamus, midbrain, and temporal cortex (T. ctx)
461 as well as B) in kidney. Red signifies the highest abundance and blue the lowest of each m/z.
462
463 **Figure S1. Phosphatidylethanolamines were not observed within parietal cortex.**
464 MALDI-IMS of SIV-infected, ART-treated rhesus macaque parietal cortex of m/z values shared
465 by PEs in linked PowerPoint file. Red signifies the highest abundance and blue the lowest of
466 each m/z.
467

468 **References**

469

470 1. M. S. Espíndola, L. S. Soares, L. J. Galvão-Lima, F. A. Zambuzi, M. C. Cacemiro, V. S.
471 Brauer, F. G. Frantz, HIV infection: focus on the innate immune cells. *Immunol Res*. 64, 1118–
472 1132 (2016).

473 2. R. W. Mitchell, G. M. Hatch, Fatty acid transport into the brain Of fatty acid fables and lipid
474 tails. *Prostaglandins, Leukotrienes and Essential Fatty Acids*. 85, 293–302 (2011).

475 3. P. A. Watkins, J. A. Hamilton, A. Leaf, A. A. Spector, S. A. Moore, R. E. Anderson, H. W.
476 Moser, M. J. Noetzel, R. Katz, (2001), vol. 16 of *Journal of molecular neuroscience : MN*, pp.
477 87-92-discussion 151-7.

478 4. A. Gongvatana, B. C. Schweinsburg, M. J. Taylor, R. J. Theilmann, S. L. Letendre, O. M.
479 Alhassoon, J. Jacobus, S. P. Woods, T. L. Jernigan, R. J. Ellis, L. R. Frank, I. Grant, T. C.
480 Group, White matter tract injury and cognitive impairment in human immunodeficiency virus–
481 infected individuals. *J Neurovirol*. 15, 187–195 (2009).

482 5. M. A. Mohamed, P. B. Barker, R. L. Skolasky, O. A. Selnes, R. T. Moxley, M. G. Pomper, N.
483 C. Sacktor, Brain metabolism and cognitive impairment in HIV infection: a 3-T magnetic
484 resonance spectroscopy study. *Magnetic Resonance Imaging*. 28, 1251–1257 (2010).

485 6. K. J. Towgood, M. Pitkanen, R. Kulasegaram, A. Fradera, S. Soni, N. Sibtain, L. J. Reed, C.
486 Bradbeer, G. J. Barker, J. T. Dunn, F. Zelaya, M. D. Kopelman, Regional cerebral blood flow
487 and FDG uptake in asymptomatic HIV-1 men. *Human Brain Mapping*. 34, 2484–2493 (2012).

488 7. T. Ernst, C. S. Jiang, H. Nakama, S. Buchthal, L. Chang, Lower brain glutamate is associated
489 with cognitive deficits in HIV patients: A new mechanism for HIV-associated neurocognitive
490 disorder. *Journal of Magnetic Resonance Imaging*. 32, 1045–1053 (2010).

491 8. Å. B. Andersen, I. Law, K. S. Krabbe, H. Bruunsgaard, S. R. Ostrowski, H. Ullum, L.
492 Højgaard, A. Lebech, J. Gerstoft, A. Kjær, Cerebral FDG-PET scanning abnormalities in
493 optimally treated HIV patients. *J Neuroinflamm*. 7, 13–13 (2010).

494 9. H. N. Consortium, A. Gongvatana, J. Harezlak, S. Buchthal, E. Daar, G. Schifitto, T.
495 Campbell, M. Taylor, E. Singer, J. Algers, J. Zhong, M. Brown, D. McMahon, Y. T. So, D. Mi, R.
496 Heaton, K. Robertson, C. Yiannoutsos, R. A. Cohen, B. Navia, Progressive cerebral injury in the
497 setting of chronic HIV infection and antiretroviral therapy. *Journal of NeuroVirology*. 19, 209–218
498 (2013).

499 10. J. J. Weiss, R. Calvi, M. Naganawa, T. Toyonaga, S. F. Farhadian, M. Chintanaphol, J.
500 Chiarella, M.-Q. Zheng, J. Ropchan, Y. Huang, R. H. Pietrzak, R. E. Carson, S. Spudich,
501 Preliminary In Vivo Evidence of Reduced Synaptic Density in Human Immunodeficiency Virus
502 (HIV) Despite Antiretroviral Therapy. *Clin Infect Dis Official Publ Infect Dis Soc Am*. 73, 1404–
503 1411 (2021).

504 11. V. Samboju, C. L. Philippi, P. Chan, Y. Cobigo, J. L. K. Fletcher, M. Robb, J. Hellmuth, K.
505 Benjapornpong, N. Dumrongpisutikul, M. Pothisri, R. Paul, J. Ananworanich, S. Spudich, V.

506 Valcour, S. 010/RV254, R. protocol teams, Structural and functional brain imaging in acute HIV.
507 *Neuroimage Clin*. 20, 327–335 (2018).

508 12. C.-X. Li, J. G. Herndon, F. J. Novembre, X. Zhang, A Longitudinal Magnetization Transfer
509 Imaging Evaluation of Brain Injury in a Macaque Model of NeuroAIDS. *Aids Res Hum Retrov*.
510 31, 335–341 (2015).

511 13. C.-X. Li, X. Zhang, A. Komery, Y. Li, H. Mao, J. G. Herndon, F. J. Novembre, Longitudinal
512 cerebral metabolic changes in pig-tailed macaques infected with the neurovirulent virus
513 SIVsmmFGb. *J Neurovirol*. 20, 612–619 (2014).

514 14. C. Li, X. Zhang, A. Komery, Y. Li, F. J. Novembre, J. G. Herndon, Longitudinal diffusion
515 tensor imaging and perfusion MRI investigation in a macaque model of neuro-AIDS: A
516 preliminary study. *Neuroimage*. 58, 286–292 (2011).

517 15. D. Saylor, A. M. Dickens, N. Sacktor, N. Haughey, B. Slusher, M. Pletnikov, J. L.
518 Mankowski, A. Brown, D. J. Volsky, J. C. McArthur, HIV-associated neurocognitive disorder —
519 pathogenesis and prospects for treatment. *Nature Reviews Neurology*. 12, 234–248 (2016).

520 16. P. Deme, C. Rojas, B. S. Slusher, R. Rais, Z. Afghah, J. D. Geiger, N. J. Haughey,
521 Bioenergetic adaptations to HIV infection. Could modulation of energy substrate utilization
522 improve brain health in people living with HIV-1? *Exp Neurol*. 327, 113181 (2020).

523 17. B. Cotto, K. Natarajaseenivasan, D. Langford, HIV-1 infection alters energy metabolism in
524 the brain:contributions to HIV-associated neurocognitive disorders. *Progress in Neurobiology*,
525 101616 (2019).

526 18. N. J. Haughey, R. G. Cutler, A. Tamara, J. C. McArthur, D. L. Vargas, C. A. Pardo, J.
527 Turchan, A. Nath, M. P. Mattson, Perturbation of sphingolipid metabolism and ceramide
528 production in HIV-dementia. *Ann Neurol*. 55, 257–267 (2004).

529 19. B. Cotto, K. Natarajaseenivasan, K. Ferrero, L. Wesley, M. Sayre, D. Langford, Cocaine and
530 HIV-1 Tat disrupt cholesterol homeostasis in astrocytes: Implications for HIV-associated
531 neurocognitive disorders in cocaine user patients. *Glia*. 66, 889–902 (2018).

532 20. K. Natarajaseenivasan, B. Cotto, S. Shanmughapriya, A. A. Lombardi, P. K. Datta, M.
533 Madesh, J. W. Elrod, K. Khalili, D. Langford, Astrocytic metabolic switch is a novel etiology for
534 Cocaine and HIV-1 Tat-mediated neurotoxicity. *Cell Death Dis*. 9, 415 (2018).

535 21. A. Y. Taha, M. Basselin, E. Ramadan, H. R. Modi, S. I. Rapoport, Y. Cheon, Altered lipid
536 concentrations of liver, heart and plasma but not brain in HIV-1 transgenic rats. *Prostaglandins*
537 *Leukot Essent Fat Acids*. 87, 91–101 (2012).

538 22. M. Vigorito, K. P. Connaghan, S. L. Chang, The HIV-1 transgenic rat model of neuroHIV.
539 *Brain Behav Immun*. 48, 336–349 (2015).

540 23. C. J. White, J. Lee, J. Choi, T. Chu, S. Scafidi, M. J. Wolfgang, Determining the Bioenergetic
541 Capacity for Fatty Acid Oxidation in the Mammalian Nervous System. *Mol Cell Biol*. 40 (2020),
542 doi:10.1128/mcb.00037-20.

543 24. G. Sighinolfi, S. Clark, L. Blanc, D. Cota, B. Rhourri-Frih, Mass spectrometry imaging of
544 mice brain lipid profile changes over time under high fat diet. *Sci Rep-uk*. 11, 19664 (2021).

545 25. J. N. Jernberg, C. E. Bowman, M. J. Wolfgang, S. Scafidi, Developmental regulation and
546 localization of carnitine palmitoyltransferases (CPTs) in rat brain. *Journal of Neurochemistry*.
547 142, 407–419 (2017).

548 26. J. N. van der Veen, J. P. Kennelly, S. Wan, J. E. Vance, D. E. Vance, R. L. Jacobs, The
549 critical role of phosphatidylcholine and phosphatidylethanolamine metabolism in health and
550 disease. *Biochimica Et Biophysica Acta Bba - Biomembr*. 1859, 1558–1572 (2017).

551 27. H.-S. Jang, M. R. Noh, J. Kim, B. J. Padanilam, Defective Mitochondrial Fatty Acid Oxidation
552 and Lipotoxicity in Kidney Diseases. *Frontiers Medicine*. 7, 65 (2020).

553 28. C. M. Abreu, R. T. Veenhuis, C. R. Avalos, S. Graham, D. R. Parrilla, E. A. Ferreira, S. E.
554 Queen, E. N. Shirk, B. T. Bullock, M. Li, K. A. M. Pate, S. E. Beck, L. M. Mangus, J. L.
555 Mankowski, F. M. Gabhann, S. L. O'Connor, L. Gama, J. E. Clements, Myeloid and CD4 T Cells
556 Comprise the Latent Reservoir in Antiretroviral Therapy-Suppressed SIVmac251-Infected
557 Macaques. *Mbio*. 10, e01659-19 (2019).

558 29. A. M. Gorska, M. Donoso, S. Valdebenito, B. Prideaux, S. Queen, E. Scemes, J. Clements,
559 E. Eugenin, Human immunodeficiency virus-1/simian immunodeficiency virus infection induces
560 opening of pannexin-1 channels resulting in neuronal synaptic compromise: A novel therapeutic
561 opportunity to prevent NeuroHIV. *J Neurochem*. 158, 500–521 (2021).

562 30. J. E. Clements, J. L. Mankowski, L. Gama, M. C. Zink, The accelerated simian
563 immunodeficiency virus macaque model of human immunodeficiency virus-associated
564 neurological disease: From mechanism to treatment. *J Neurovirol*. 14, 309–317 (2008).

565 31. G. M. Shaw, M. E. Harper, B. H. Hahn, L. G. Epstein, D. C. Gajdusek, R. W. Price, B. A.
566 Navia, C. K. Petito, C. J. O'Hara, J. E. Groopman, E.-S. Cho, J. M. Oleske, F. Wong-Staal, R.
567 C. Gallo, HTLV-III Infection in Brains of Children and Adults with AIDS Encephalopathy.
568 *Science*. 227, 177–182 (1985).

569 32. J. Rappaport, D. J. Volsky, Role of the macrophage in HIV-associated neurocognitive
570 disorders and other comorbidities in patients on effective antiretroviral treatment. *J Neurovirol*.
571 21, 235–241 (2015).

572 33. K. Williams, S. Westmoreland, J. Greco, E. Ratai, M. Lentz, W.-K. Kim, R. A. Fuller, J. P.
573 Kim, P. Autissier, P. K. Sehgal, R. F. Schinazi, N. Bischofberger, M. Piatak, J. D. Lifson, E.
574 Masliah, R. G. González, Magnetic resonance spectroscopy reveals that activated monocytes
575 contribute to neuronal injury in SIV neuroAIDS. *J Clin Invest*. 115, 2534–2545 (2005).

576 34. V. Monceaux, L. Viollet, F. Petit, M. C. Cumont, G. R. Kaufmann, A. M. Aubertin, B. Hurtrel,
577 G. Silvestri, J. Estaquier, CD4 + CCR5 + T-Cell Dynamics during Simian Immunodeficiency
578 Virus Infection of Chinese Rhesus Macaques. *J Virol*. 81, 13865–13875 (2007).

579 35. J. B. Whitney, A. L. Hill, S. Sanisetty, P. Penaloza-MacMaster, J. Liu, M. Shetty, L.
580 Parenteau, C. Cabral, J. Shields, S. Blackmore, J. Y. Smith, A. L. Brinkman, L. E. Peter, S. I.
581 Mathew, K. M. Smith, E. N. Borducchi, D. I. S. Rosenbloom, M. G. Lewis, J. Hattersley, B. Li, J.

582 Hesselgesser, R. Geleziunas, M. L. Robb, J. H. Kim, N. L. Michael, D. H. Barouch, Rapid
583 Seeding of the Viral Reservoir Prior to SIV Viremia in Rhesus Monkeys. *Nature*. 512, 74–77
584 (2014).

585 36. S. Tuyishime, L. H. Haut, R. K. Kurupati, J. M. Billingsley, D. Carnathan, S. Gangahara, T.
586 M. Styles, Z. Xiang, Y. Li, M. Zopfs, Q. Liu, X. Zhou, M. G. Lewis, R. R. Amara, S. Bosinger, G.
587 Silvestri, H. C. J. Ertl, Correlates of Protection Against SIVmac251 Infection in Rhesus
588 Macaques Immunized With Chimpanzee-Derived Adenovirus Vectors. *Ebiomedicine*. 31, 25–35
589 (2018).

590 37. D. H. Barouch, G. Alter, T. Broge, C. Linde, M. E. Ackerman, E. P. Brown, E. N. Borducchi,
591 K. M. Smith, J. P. Nkolola, J. Liu, J. Shields, L. Parenteau, J. B. Whitney, P. Abbink, D. M.
592 Ng'ang'a, M. S. Seaman, C. L. Lavine, J. R. Perry, W. Li, A. D. Colantonio, M. G. Lewis, B.
593 Chen, H. Wenschuh, U. Reimer, M. Piatak, J. D. Lifson, S. A. Handley, H. W. Virgin, M.
594 Koutsoukos, C. Lorin, G. Voss, M. Weijtens, M. G. Pau, H. Schuitemaker, Protective efficacy of
595 adenovirus/protein vaccines against SIV challenges in rhesus monkeys. *Science*. 349, 320–324
596 (2015).

597 38. D. H. Barouch, P. J. Klasse, J. Dufour, R. S. Veazey, J. P. Moore, Macaque studies of
598 vaccine and microbicide combinations for preventing HIV-1 sexual transmission. *Proc National*
599 *Acad Sci*. 109, 8694–8698 (2012).

600 39. M. Vaccari, B. F. Keele, S. E. Bosinger, M. N. Doster, Z.-M. Ma, J. Pollara, A. Hryniewicz, G.
601 Ferrari, Y. Guan, D. N. Forthal, D. Venzon, C. Fenizia, T. Morgan, D. Montefiori, J. D. Lifson, C.
602 J. Miller, G. Silvestri, M. Rosati, B. K. Felber, G. N. Pavlakis, J. Tartaglia, G. Franchini,
603 Protection Afforded by an HIV Vaccine Candidate in Macaques Depends on the Dose of SIV
604 mac251 at Challenge Exposure. *J Virol*. 87, 3538–3548 (2013).

605 40. L. Micci, X. Alvarez, R. I. Iriele, A. M. Ortiz, E. S. Ryan, C. S. McGary, C. Deleage, B. B.
606 McAtee, T. He, C. Apetrei, K. Easley, S. Pahwa, R. G. Collman, C. A. Derdeyn, M. P.
607 Davenport, J. D. Estes, G. Silvestri, A. A. Lackner, M. Paiardini, CD4 Depletion in SIV-Infected
608 Macaques Results in Macrophage and Microglia Infection with Rapid Turnover of Infected Cells.
609 *Plos Pathog*. 10, e1004467 (2014).

610 41. B. R. Magalis, D. J. Nolan, P. Autissier, T. H. Burdo, K. C. Williams, M. Salemi, Insights into
611 the Impact of CD8 + Immune Modulation on Human Immunodeficiency Virus Evolutionary
612 Dynamics in Distinct Anatomical Compartments by Using Simian Immunodeficiency Virus-
613 Infected Macaque Models of AIDS Progression. *J Virol*. 91 (2017), doi:10.1128/jvi.01162-17.

614 42. J. Mallard, K. C. Williams, Chapter 4 Animal models of HIV-associated disease of the central
615 nervous system. *Handb Clin Neurology*. 152, 41–53 (2018).

616 43. M. R. Lentz, S. V. Westmoreland, V. Lee, E. Ratai, E. F. Halpern, R. G. González, Metabolic
617 markers of neuronal injury correlate with SIV CNS disease severity and inoculum in the
618 macaque model of neuroAIDS. *Magnet Reson Med*. 59, 475–484 (2008).

619 44. A. Shen, M. C. Zink, J. L. Mankowski, K. Chadwick, J. B. Margolick, L. M. Carruth, M. Li, J.
620 E. Clements, R. F. Siliciano, Resting CD4 + T Lymphocytes but Not Thymocytes Provide a
621 Latent Viral Reservoir in a Simian Immunodeficiency Virus- Macaca nemestrina Model of

622 Human Immunodeficiency Virus Type 1-Infected Patients on Highly Active Antiretroviral
623 Therapy. *J Virol*. 77, 4938–4949 (2003).

624 45. L. Gama, E. N. Shirk, J. N. Russell, K. I. Carvalho, M. Li, S. E. Queen, J. Kalil, M. C. Zink, J.
625 E. Clements, E. G. Kallas, Expansion of a subset of CD14highCD16negCCR2low/neg
626 monocytes functionally similar to myeloid-derived suppressor cells during SIV and HIV infection.
627 *J Leukocyte Biol*. 91, 803–816 (2012).

628 46. L. Gama, C. M. Abreu, E. N. Shirk, S. L. Price, M. Li, G. M. Laird, K. A. M. Pate, S. W.
629 Wietgrefe, S. L. O'Connor, L. Pianowski, A. T. Haase, C. V. Lint, R. F. Siliciano, J. E. Clements,
630 Reactivation of simian immunodeficiency virus reservoirs in the brain of virally suppressed
631 macaques. *Aids*. 31, 5–14 (2017).

632 47. K. A. Meulendyke, M. V. Pletnikov, E. L. Engle, P. M. Tarwater, D. R. Graham, M. C. Zink,
633 Early Minocycline Treatment Prevents a Decrease in Striatal Dopamine in an SIV Model of HIV-
634 Associated Neurological Disease. *J Neuroimmune Pharm*. 7, 454–464 (2012).

635 48. M. C. Zink, K. Suryanarayana, J. L. Mankowski, A. Shen, M. Piatak, J. P. Spelman, D. L.
636 Carter, R. J. Adams, J. D. Lifson, J. E. Clements, High Viral Load in the Cerebrospinal Fluid and
637 Brain Correlates with Severity of Simian Immunodeficiency Virus Encephalitis. *J Virol*. 73,
638 10480–10488 (1999).

639 49. K. C. Pathmasiri, T. T. A. Nguyen, N. Khamidova, S. M. Cologna, Mass spectrometry-based
640 lipid analysis and imaging. *Curr Top Membr*. 88, 315–357 (2021).

641 50. E. Fahy, S. Subramaniam, R. C. Murphy, M. Nishijima, C. R. H. Raetz, T. Shimizu, F.
642 Spener, G. van Meer, M. J. O. Wakelam, E. A. Dennis, Update of the LIPID MAPS
643 comprehensive classification system for lipids 1. *J Lipid Res*. 50, S9–S14 (2009).

644 51. D. A. Lewis, The Human Brain Revisited: Opportunities and Challenges in Postmortem
645 Studies of Psychiatric Disorders. *Neuropsychopharmacol*. 26, 143–154 (2002).

646 52. J. Weickenmeier, M. Kurt, E. Ozkaya, R. de Rooij, T. C. Ovaert, R. L. Ehman, K. B. Pauly,
647 E. Kuhl, Brain stiffens post mortem. *J Mech Behav Biomed*. 84, 88–98 (2018).

648 53. A. C. Birdsill, D. G. Walker, L. Lue, L. I. Sue, T. G. Beach, Postmortem interval effect on
649 RNA and gene expression in human brain tissue. *Cell Tissue Bank*. 12, 311–318 (2011).

650 54. Z. ElHajj, A. Cachot, T. Müller, I. M. Riederer, B. M. Riederer, Effects of postmortem delays
651 on protein composition and oxidation. *Brain Res Bull*. 121, 98–104 (2016).

652 55. R. W. Mitchell, N. H. On, M. R. D. Bigio, D. W. Miller, G. M. Hatch, Fatty acid transport
653 protein expression in human brain and potential role in fatty acid transport across human brain
654 microvessel endothelial cells. *J Neurochem*. 117, 735–746 (2011).

655 56. A. T. Ahmed, S. MahmoudianDehkordi, S. Bhattacharyya, M. Arnold, D. Liu, D. Neavin, M.
656 A. Moseley, J. W. Thompson, L. S. J. Williams, G. Louie, M. K. Skime, L. Wang, P. Riva-Posse,
657 W. McDonald, W. V. Bobo, W. E. Craighead, R. Krishnan, R. M. Weinshilboum, B. W. Dunlop,
658 D. S. Millington, A. J. Rush, M. A. Frye, R. Kaddurah-Daouk, T. M. D. P. M. C. (MDPMC),

659 Acylcarnitine metabolomic profiles inform clinically-defined major depressive phenotypes. *J*
660 *Affect Disorders*. 264, 90–97 (2020).

661 57. T. Clark-Taylor, B. E. Clark-Taylor, Is autism a disorder of fatty acid metabolism? Possible
662 dysfunction of mitochondrial β-oxidation by long chain acyl-CoA dehydrogenase. *Medical*
663 *Hypotheses*. 62, 970–975 (2004).

664 58. R. Barone, S. Alaimo, M. Messina, A. Pulvirenti, J. Bastin, M.-A. Group, A. Ferro, R. E. Frye,
665 R. Rizzo, A Subset of Patients With Autism Spectrum Disorders Show a Distinctive Metabolic
666 Profile by Dried Blood Spot Analyses. *Frontiers in Psychiatry*. 9, 1–11 (2018).

667 59. C. M. Wyatt, Kidney Disease and HIV Infection. *Top Antivir Medicine*. 25, 13–16 (2017).

668 60. C. C. C. R. de Carvalho, M. J. Caramujo, The Various Roles of Fatty Acids. *Mol J Synthetic*
669 *Chem Nat Prod Chem*. 23, 2583 (2018).

670 61. S. Iskander, K. A. Walsh, R. R. Hammond, Human CNS cultures exposed to HIV-1 gp120
671 reproduce dendritic injuries of HIV-1-associated dementia. *J Neuroinflamm*. 1, 7 (2004).

672 62. S. M. Toggas, E. Masliah, E. M. Rockenstein, G. F. Rail, C. R. Abraham, L. Mucke, Central
673 nervous system damage produced by expression of the HIV-1 coat protein gpl20 in transgenic
674 mice. *Nature*. 367, 188–193 (1994).

675 63. B. O. Kim, Y. Liu, Y. Ruan, Z. C. Xu, L. Schantz, J. J. He, Neuropathologies in Transgenic
676 Mice Expressing Human Immunodeficiency Virus Type 1 Tat Protein under the Regulation of
677 the Astrocyte-Specific Glial Fibrillary Acidic Protein Promoter and Doxycycline. *Am J Pathology*.
678 162, 1693–1707 (2003).

679 64. R. Putatunda, Y. Zhang, F. Li, X.-F. Yang, M. F. Barbe, W. Hu, Adult neurogenic deficits in
680 HIV-1 Tg26 transgenic mice. *J Neuroinflamm*. 15, 287 (2018).

681 65. M. F. Salahuddin, F. Mahdi, S. P. Sulochana, J. J. Paris, HIV-1 Tat Protein Promotes
682 Neuroendocrine Dysfunction Concurrent with the Potentiation of Oxycodone's Psychomotor
683 Effects in Female Mice. *Viruses*. 13, 813 (2021).

684 66. A. Nath, J. Geiger, Neurobiological aspects of human immunodeficiency virus
685 infection:Neurotoxic mechanisms. *Prog Neurobiol*. 54, 19–33 (1998).

686 67. V. Repunte-Canonigo, C. Lefebvre, O. George, T. Kawamura, M. Morales, G. F. Koob, A.
687 Califano, E. Masliah, P. P. Sanna, Gene expression changes consistent with neuroAIDS and
688 impaired working memory in HIV-1 transgenic rats. *Mol Neurodegener*. 9, 26–26 (2014).

689 68. S. Fitting, P. E. Knapp, S. Zou, W. D. Marks, M. S. Bowers, H. I. Akbarali, K. F. Hauser,
690 Interactive HIV-1 Tat and Morphine-Induced Synaptodendritic Injury Is Triggered through Focal
691 Disruptions in Na+ Influx, Mitochondrial Instability, and Ca2+ Overload. *J Neurosci*. 34, 12850–
692 12864 (2014).

693 69. S. Fitting, S. Zou, N. El-Hage1, M. Suzuki, J. J. Paris, C. J. Schier, J. W. Rodríguez, M.
694 Rodriguez, P. E. Knapp, K. F. Hauser, Opiate Addiction Therapies and HIV-1 Tat: Interactive

695 Effects on Glial [Ca2+]i, Oxyradical and Neuroinflammatory Chemokine Production and
696 Correlative Neurotoxicity. *Curr Hiv Res*. 12, 424–434 (2014).

697 70. A. Ciardo, J. Meldolesi, Effects of the HIV-1 Envelope Glycoprotein gp120 in Cerebellar
698 Cultures. [Ca2+]i Increases in a Glial Cell Subpopulation. *Eur J Neurosci*. 5, 1711–1718 (1993).

699 71. L. M. Villeneuve, P. R. Purnell, K. L. Stauch, S. E. Callen, S. J. Buch, H. S. Fox, HIV-1
700 transgenic rats display mitochondrial abnormalities consistent with abnormal energy generation
701 and distribution. *Journal of NeuroVirology*, 1–11 (2016).

702 72. J. Steiner, N. Haughey, W. Li, A. Venkatesan, C. Anderson, R. Reid, T. Malpica, C.
703 Pocernich, D. A. Butterfield, A. Nath, Oxidative Stress and Therapeutic Approaches in HIV
704 Dementia. *Antioxid Redox Sign*. 8, 2089–2100 (2006).

705 73. L. Agrawal, J.-P. Louboutin, E. Marusich, B. A. S. Reyes, E. J. V. Bockstaele, D. S. Strayer,
706 Dopaminergic neurotoxicity of HIV-1 gp120: Reactive oxygen species as signaling
707 intermediates. *Brain Res*. 1306, 116–130 (2010).

708 74. G. J. Jones, N. L. Barsby, E. A. Cohen, J. Holden, K. Harris, P. Dickie, J. Jhamandas, C.
709 Power, HIV-1 Vpr Causes Neuronal Apoptosis and In Vivo Neurodegeneration. *J Neurosci*. 27,
710 3703–3711 (2007).

711 75. P. Duffau, A. Ozanne, F. Bonnet, E. Lazaro, C. Cazanave, P. Blanco, E. Rivière, A.
712 Desclaux, C. Hyernard, N. Gensous, I. Pellegrin, L. Wittkop, Multimorbidity, age-related
713 comorbidities and mortality. *Aids*. 32, 1651–1660 (2018).

714 76. A. Edén, T. D. Marcotte, R. K. Heaton, S. Nilsson, H. Zetterberg, D. Fuchs, D. Franklin, R.
715 W. Price, I. Grant, S. L. Letendre, M. Gisslén, Increased Intrathecal Immune Activation in Virally
716 Suppressed HIV-1 Infected Patients with Neurocognitive Impairment. *Plos One*. 11, e0157160
717 (2016).

718 77. A. Winston, S. Spudich, Cognitive disorders in people living with HIV. *Lancet Hiv*. 7, e504–
719 e513 (2020).

720 78. R. T. Veenhuis, D. W. Williams, E. N. Shirk, C. M. Abreu, E. A. Ferreira, J. M. Coughlin, T.
721 T. Brown, P. M. Maki, K. Anastos, J. W. Berman, J. E. Clements, L. H. Rubin, Higher circulating
722 intermediate monocytes are associated with cognitive function in women with HIV. *Jci Insight*
723 (2021), doi:10.1172/jci.insight.146215.

724 79. A. C. Vecchio, D. W. Williams, Y. Xu, D. Yu, D. Saylor, S. Lofgren, R. O'Toole, D. R.
725 Boulware, N. Nakasujja, G. Nakigozi, A. Kisakye, J. Batte, R. Mayanja, A. Anok, S. J. Reynolds,
726 T. C. Quinn, R. H. Gray, M. J. Wawer, N. Sacktor, L. H. Rubin, Sex-specific associations
727 between cerebrospinal fluid inflammatory marker levels and cognitive function in antiretroviral
728 treated people living with HIV in rural Uganda. *Brain Behav Immun*. 93, 111–118 (2021).

729 80. L. H. Rubin, Y. Xu, P. J. Norris, X. Wang, R. Dastgheyb, K. C. Fitzgerald, S. M. Keating, R.
730 C. Kaplan, P. M. Maki, K. Anastos, G. Springer, L. Benning, S. Kassaye, D. R. Gustafson, V. G.
731 Valcour, D. W. Williams, Early Inflammatory Signatures Predict Subsequent Cognition in Long-
732 Term Virally Suppressed Women With HIV. *Frontiers Integr Neurosci*. 14, 20 (2020).

733 81. A. R. Kamkwalala, X. Wang, P. M. Maki, D. W. Williams, V. G. Valcour, A. Damron, P. C.
734 Tien, K. M. Weber, M. H. Cohen, E. E. Sundermann, V. J. Meyer, D. M. Little, Y. Xu, L. H.
735 Rubin, Brief Report: Higher Peripheral Monocyte Activation Markers Are Associated With
736 Smaller Frontal and Temporal Cortical Volumes in Women With HIV. *J Acquir Immune Defic*
737 *Syndromes 1999*. 84, 54–59 (2020).

738 82. D. W. Williams, D. Byrd, L. H. Rubin, K. Anastos, S. Morgello, J. W. Berman, CCR2 on
739 CD14(+)CD16(+) monocytes is a biomarker of HIV-associated neurocognitive disorders.
740 *Neurology Neuroimmunol Neuroinflammation*. 1, e36 (2014).

741 83. M. Deleidi, M. Jäggle, G. Rubino, Immune aging, dysmetabolism, and inflammation in
742 neurological diseases. *Front Neurosci-switz*. 9, 172 (2015).

743 84. T. Shabab, R. Khanabdali, S. Z. Moghadamtousi, H. A. Kadir, G. Mohan, Neuroinflammation
744 pathways: a general review. *Int J Neurosci*. 127, 1–10 (2016).

745 85. S. G. Fard, D. Cameron-Smith, A. J. Sinclair, n – 3 Docosapentaenoic acid: the iceberg n –
746 3 fatty acid. *Curr Opin Clin Nutrition Metabolic Care*. 24, 134–138 (2020).

747 86. M. Sapuła, M. Suchacz, A. Załęski, A. Wiercińska-Drapało, Impact of Combined
748 Antiretroviral Therapy on Metabolic Syndrome Components in Adult People Living with HIV: A
749 Literature Review. *Viruses*. 14, 122 (2022).

750 87. K. Bourgi, C. A. Jenkins, P. F. Rebeiro, B. E. Shepherd, F. Palella, R. D. Moore, K. N.
751 Althoff, J. Gill, C. S. Rabkin, S. J. Gange, M. A. Horberg, J. Margolick, J. Li, C. Wong, A. Willig,
752 V. D. Lima, H. Crane, J. Thorne, M. Silverberg, G. Kirk, W. C. Mathews, T. R. Sterling, J. Lake,
753 J. R. Koethe, for the N. A. A. C. C. on R. and D. (NA-ACCORD), Weight gain among treatment-
754 naïve persons with HIV starting integrase inhibitors compared to non-nucleoside reverse
755 transcriptase inhibitors or protease inhibitors in a large observational cohort in the United States
756 and Canada. *J Int Aids Soc*. 23, e25484 (2020).

757 88. P. E. Sax, K. M. Erlandson, J. E. Lake, G. A. McComsey, C. Orkin, S. Esser, T. T. Brown, J.
758 K. Rockstroh, X. Wei, C. C. Carter, L. Zhong, D. M. Brainard, K. Melbourne, M. Das, H.-J.
759 Stellbrink, F. A. Post, L. Waters, J. R. Koethe, Weight Gain Following Initiation of Antiretroviral
760 Therapy: Risk Factors in Randomized Comparative Clinical Trials. *Clin Infect Dis*. 71, 1379–
761 1389 (2019).

762 89. H. Stires, J. LaMori, W. Chow, Z. Zalewski, A. Vidulich, M. Avina, C. Sloan, R. Hughes, H.
763 Hardy, Weight Gain and Related Comorbidities Following Antiretroviral Initiation in the 2000s: A
764 Systematic Literature Review. *Aids Res Hum Retrov*. 37, 834–841 (2021).

765 90. D. M. Byonanebye, R. S. Group, Incidence of dyslipidemia in people with HIV who are
766 treated with integrase inhibitors versus other antiretroviral agents. *Aids*. 35, 869–882 (2021).

767 91. P.-E. Plum, N. Maes, A.-S. Sauvage, F. Frippiat, C. Meuris, F. Uurlings, M. Lecomte, P.
768 Léonard, N. Paquot, K. Fombellida, D. Vaira, M. Moutschen, G. Darcis, Impact of switch from
769 tenofovir disoproxil fumarate-based regimens to tenofovir alafenamide-based regimens on lipid
770 profile, weight gain and cardiovascular risk score in people living with HIV. *Bmc Infect Dis*. 21,
771 910 (2021).

92. J. Lagoutte-Renosi, M. Flammang, C. Chirouze, G. Beck-Wirth, F. Bozon, A.-S. Brunel, M.-C. Drobacheff-Thiebaut, A. Foltzer, L. Hustache-Mathieu, J. Kowalczyk, C. Michel, S. Davani, P. Muret, Real-Life Impact on Lipid Profile of a Switch from Tenofovir Disoproxil Fumarate to Tenofovir Alafenamide in HIV-Infected Patients. *Curr Hiv Res*. 19, 84–89 (2021).

93. W. El-Sadr, C. Mullin, A. Carr, C. Gibert, C. Rappoport, F. Visnegarwala, C. Grunfeld, S. Raghavan, Effects of HIV disease on lipid, glucose and insulin levels: results from a large antiretroviral-naïve cohort. *Hiv Med*. 6, 114–121 (2005).

94. N. T. Funderburg, N. N. Mehta, Lipid Abnormalities and Inflammation in HIV Inflection. *Curr Hiv-aids Rep*. 13, 218–225 (2016).

95. S. D. Yacovo, M. Saumoy, J. L. Sánchez-Quesada, A. Navarro, D. Sviridov, M. Javaloyas, R. Vila, A. Vernet, H. Low, J. Peñafiel, B. García, J. Ordoñez-Llanos, D. Podzamczer, Lipids, biomarkers, and subclinical atherosclerosis in treatment-naive HIV patients starting or not starting antiretroviral therapy: Comparison with a healthy control group in a 2-year prospective study. *Plos One*. 15, e0237739 (2020).

96. M. Saumoy, J. L. Sanchez-Quesada, J. Ordoñez-Llanos, D. Podzamczer, Do All Integrase Strand Transfer Inhibitors Have the Same Lipid Profile? Review of Randomised Controlled Trials in Naïve and Switch Scenarios in HIV-Infected Patients. *J Clin Medicine*. 10, 3456 (2021).

97. C. U. Nduka, S. Stranges, A. M. Sarki, P. K. Kimani, O. A. Uthman, Evidence of increased blood pressure and hypertension risk among people living with HIV on antiretroviral therapy: a systematic review with meta-analysis. *J Hum Hypertens*. 30, 355–362 (2016).

98. X. Zhao, K. Sun, Z. Lan, W. Song, L. Cheng, W. Chi, J. Chen, Y. Huo, L. Xu, X. Liu, H. Deng, J. A. Siegenthaler, L. Chen, Tenofovir and adefovir down-regulate mitochondrial chaperone TRAP1 and succinate dehydrogenase subunit B to metabolically reprogram glucose metabolism and induce nephrotoxicity. *Sci Rep-uk*. 7, 46344 (2017).

99. M. Ikeda, Y. Wakabayashi, K. Okamoto, S. Yanagimoto, S. Okugawa, K. Moriya, Changing trends in lipid profile and biomarkers of renal function and bone metabolism before and after switching from tenofovir disoproxil fumarate to tenofovir alafenamide: a prospective observational study. *Aids Res Ther*. 18, 30 (2021).

802 Figure 1.

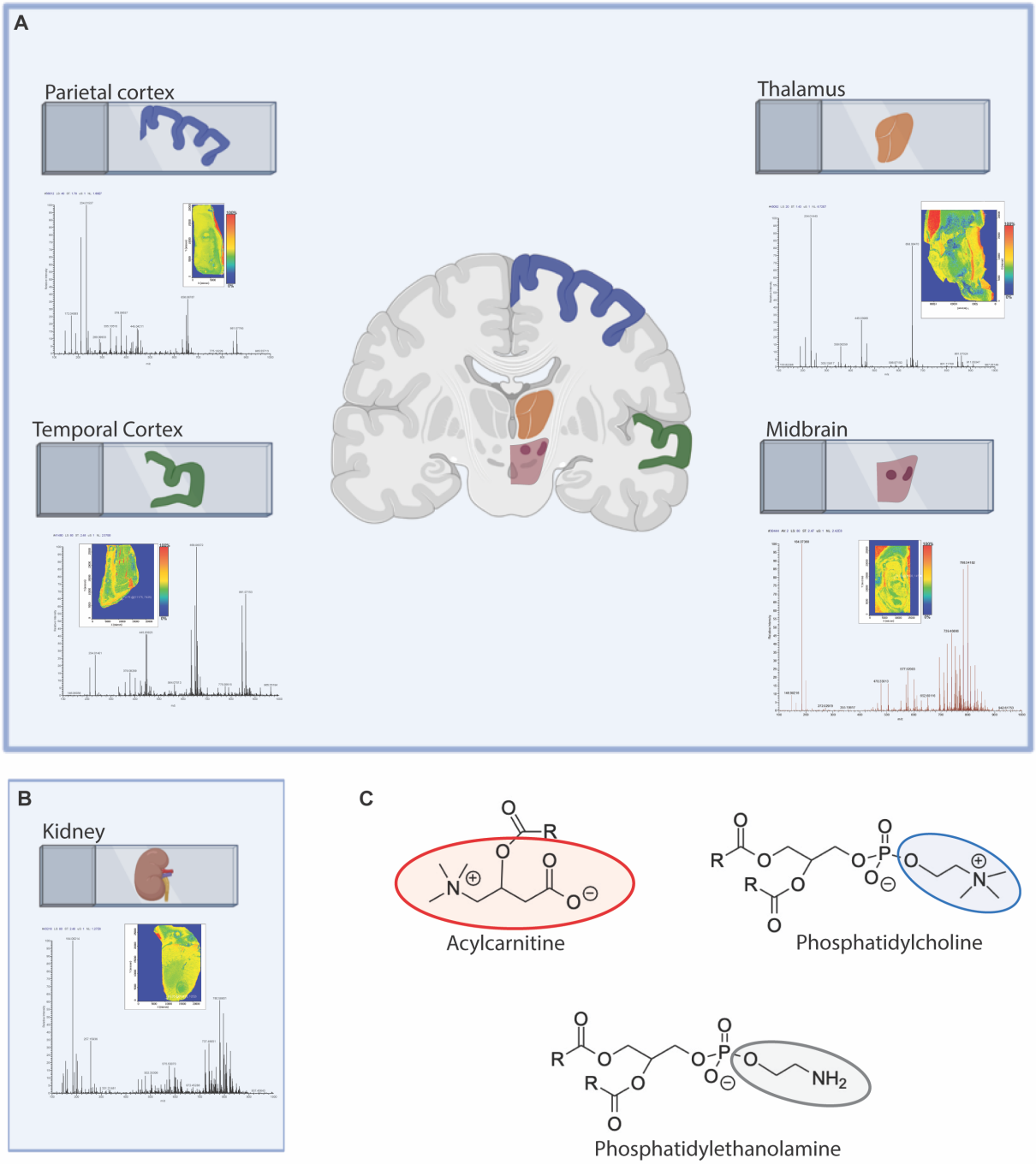

803

804

Figure 2.

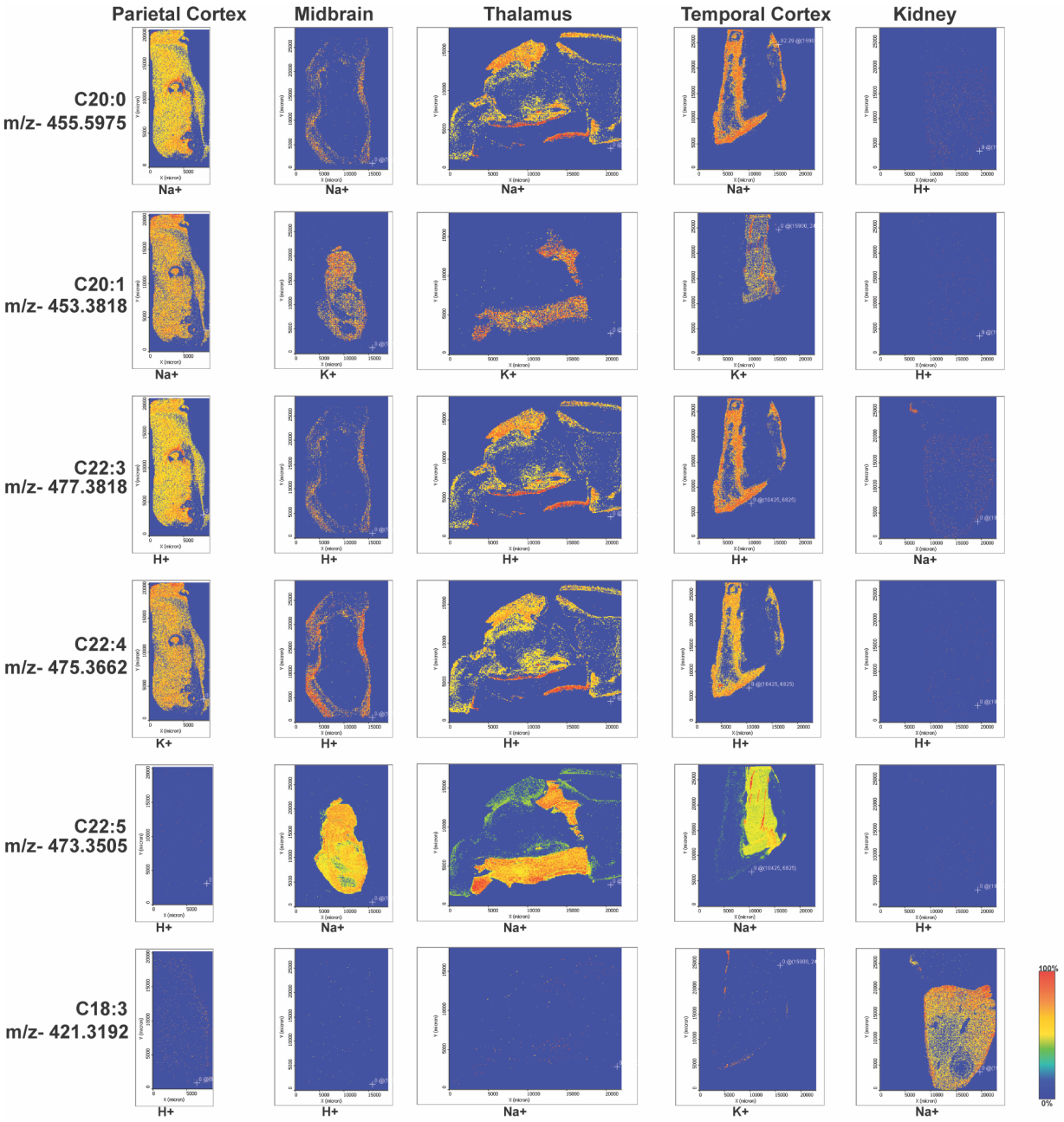
Parietal Cortex
Midbrain
Thalamus
Temporal Cortex
Kidney
C20:0
m/z- 455.5975
Na+
Na+
Na+
Na+
H+
C20:1
m/z- 453.3818
Na+
K+
K+
K+
H+
C22:3
m/z- 477.3818
H+
H+
H+
H+
Na+
C22:4
m/z- 475.3662
K+
H+
H+
H+
H+
C22:5
m/z- 473.3505
H+
Na+
Na+
Na+
H+
C18:3
m/z- 421.3192
H+
H+
Na+
K+
Na+
100%
0%

808 Figure 3.

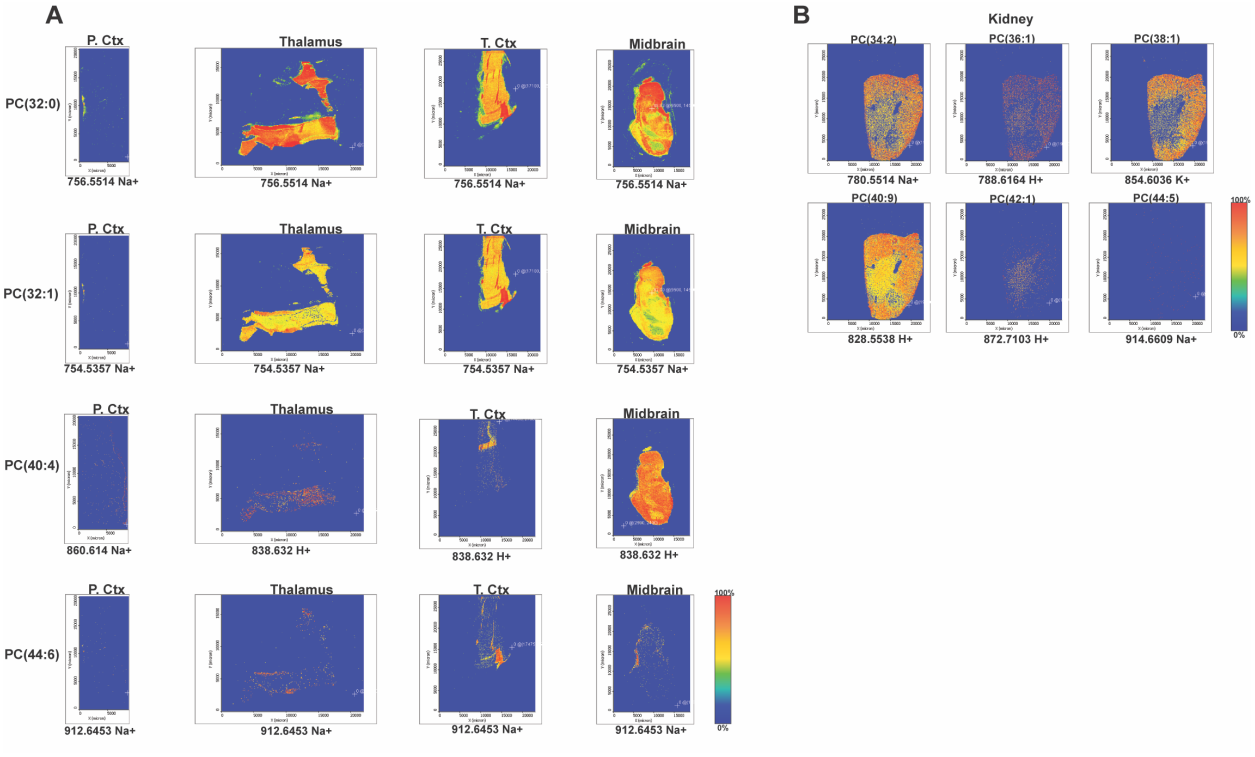

809

810

Figure 4.

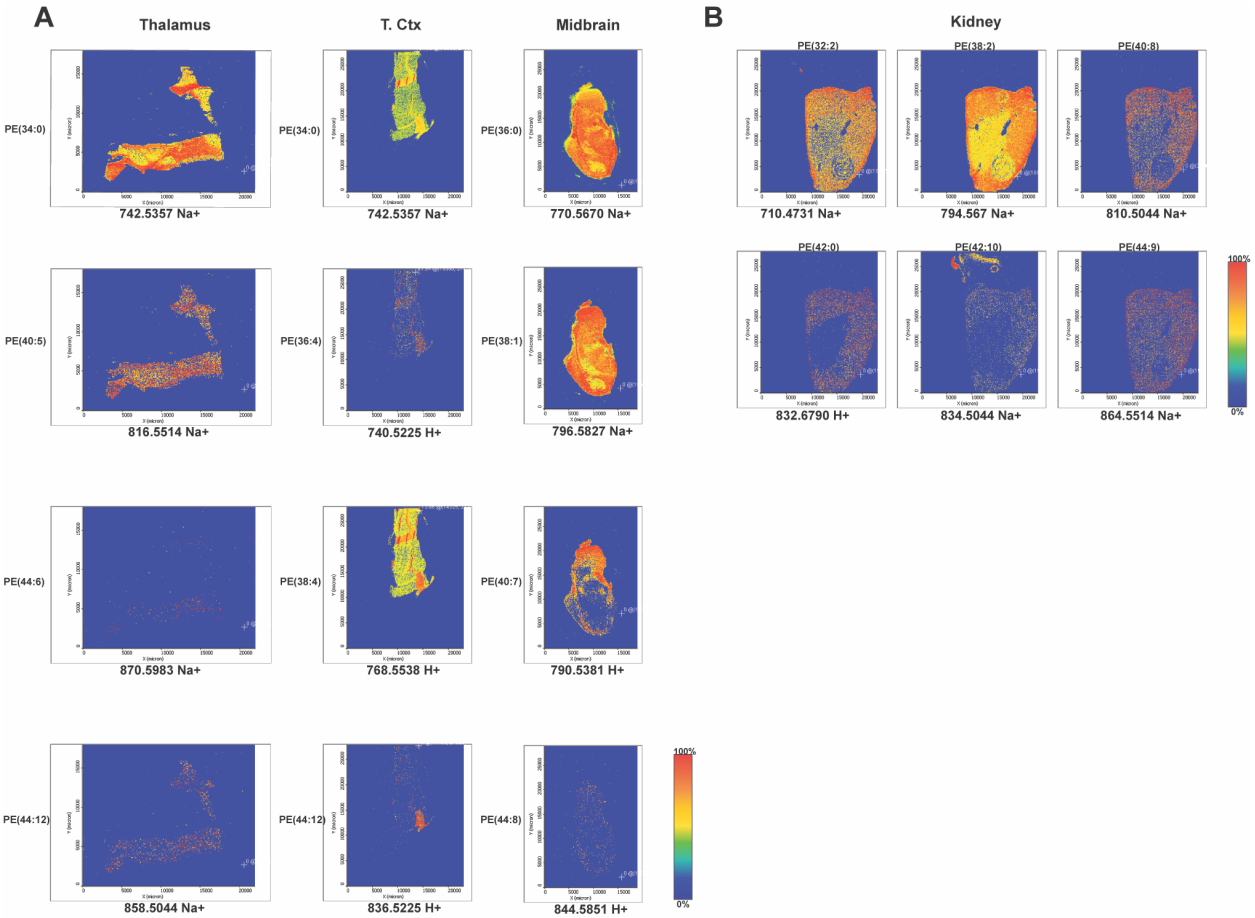
A
Thalamus
T. Ctx
Midbrain
PE(34:0)
742.5357 Na+
PE(34:0)
742.5357 Na+
PE(36:0)
770.5670 Na+
PE(40:5)
816.5514 Na+
PE(36:4)
740.5225 H+
PE(38:1)
796.5827 Na+
PE(44:6)
870.5983 Na+
PE(38:4)
768.5538 H+
PE(40:7)
790.5381 H+
PE(44:12)
858.5044 Na+
PE(44:12)
836.5225 H+
PE(44:8)
844.5851 H+
100%
0%
B
Kidney
PE(32:2)
710.4731 Na+
PE(38:2)
794.567 Na+
PE(40:8)
810.5044 Na+
PE(42:0)
832.6790 H+
PE(42:10)
834.5044 Na+
PE(44:9)
864.5514 Na+
100%
0%